Transfer between the cesium $6\,^2P_{1/2}$ and $6\,^2P_{3/2}$ levels induced by collisions with H_2, HD, D_2, CH_4, C_2H_6, CF_4, and C_2F_6

Greg A. Pitz*
Directed Energy Directorate, Air Force Research Labs, 3550 Aberdeen Ave. SE, Kirtland AFB, New Mexico 87117, USA

Charles D. Fox and Glen P. Perram†
Department of Engineering Physics, The Air Force Institute of Technology, 2950 Hobson Way, WPAFB, Ohio 45433-7765, USA

(Received 4 April 2011; published 12 September 2011)

The cross sections of spin-orbit energy exchange between the cesium $6\,^2P_{1/2} \leftrightarrow 6\,^2P_{3/2}$ states induced by collisions with N_2, H_2, HD, D_2, CH_4, C_2H_6, CF_4, and C_2F_6 were obtained for pressures less than 100 Torr at room temperature by means of steady-state laser-induced fluorescence techniques. The spin-orbit energy exchange rate with N_2, H_2, HD, D_2, CH_4, C_2H_6, CF_4, and C_2F_6, have been measured as $\sigma_{21}(6\,^2P_{3/2} \rightarrow 6\,^2P_{1/2}) = 16.3$, 34.1, 30.0, 22.7, 21.4, 65.6, 64.8, and 137 Å^2 and $\sigma_{12}(6\,^2P_{1/2} \rightarrow 6\,^2P_{3/2}) = 1.8$, 4.4, 4.1, 3.0, 2.9, 13.3, 9.7, and 16.3 Å^2, respectively. Correlations of the spin-orbit transfer probabilities with rotational-energy defect and vibrational-energy defect have been shown.

DOI: 10.1103/PhysRevA.84.032708 PACS number(s): 34.50.Ez, 42.55.Xi, 42.55.Lt

I. INTRODUCTION

Since the 1960s, collision-induced mixing between the $^2P_{1/2,3/2}$ states of alkalis have been thoroughly studied [1–9]. These mixing rates have again become of keen interest because of their role in diode-pumped alkali-metal lasers (DPAL). The DPAL system was first demonstrated by Krupke and Beach [10,11]. This alkali-metal laser can be considered an adaptation of the laser system proposed in 1958 by Schawlow and Townes [12]. The DPAL system is a three-level laser system that is pumped by diode bars or stacks along the D_2 transition to its $^2P_{3/2}$ state, then collisionally relaxed to the $^2P_{1/2}$ state where it lases down the D_1 transition. Recent demonstrations have employed ethane and methane as the collisional partner for spin-orbit relaxation. While ethane has an excellent rate for energy transfer, it also degrades laser performance with the production of laser snow and soot [13,14]. Hydrocarbon-free lasers have recently been demonstrated for both potassium and rubidium using rare-gas collision partners [15]. For cesium, the larger spin-orbit splitting requires molecular collision partners [14].

The most recent study of the mixing rate between the cesium $6\,^2P_{1/2} \leftrightarrow 6\,^2P_{3/2}$ states was performed in 1974 by Walentynowicz [7,8]. In that investigation, a cesium discharge lamp was used to excite the desired states in cesium with a pair of photomultiplier tubes to monitor the fluorescence of the two mixing states. In addition, Walentynowicz assumed quenching was negligible and observed the resulting intensities at several different pressures of no more than 1.5 Torr. Revisiting the cesium rates using laser-based methods and continuous variation of buffer gas pressures offer significant improvements in the signal-to-noise ratios and allows for lower alkali-metal densities avoiding optically trapped conditions.

The rates for fine-structure mixing in the alkali metals for collisions with rare-gas partners decrease with adiabaticity [2]. The higher relative speed of the lighter rare gases shortens the collision duration. The rubidium–rare-gas potentials exhibit interaction lengths of 0.3–0.7 nm, suggesting interaction times of $\tau_c = (0.2{-}2.0) \times 10^{-12}$ s. The fine-structure splitting increases for the heavier alkali-metal atoms: $\Delta E =$ 57.7, 237.6, and 554 cm^{-1} for K, Rb, and Cs, respectively. The corresponding oscillation periods, $\tau_{so} = \hbar/\Delta E$ decrease from 10^{-13} s for K to 10^{-14} s for Cs. The collisions are nearly adiabatic, $\xi = \tau_c/\tau_{so} = 2{-}200$, and the rates are low. The scaling of the rates with rare-gas mass, alkali-metal fine-structure splitting, and gas temperature all support adiabaticity controlling the rate [2]. Only Li and Na approach the sudden limit.

The scaling of relaxation rates with molecular collision partners is less clear. A rotational energy-transfer mechanism has been suggested for rubidium [9]. Indeed, the rates increase when the fine-structure splitting and available rovibrational excitation in the collision partner are matched [9]. In the present work we explore the role of energy transfer for the larger fine-structure splitting in Cs. The spin-orbit mixing rate between the $6\,^2P_{3/2}$ and the $6\,^2P_{1/2}$ levels of cesium caused by collision with N_2, H_2, HD, D_2, CH_4, CF_4, and C_2H_6 over a continuous range of 0–100 Torr are observed. Quenching rates are also reported from the high pressure limit. The role of the energy defect between cesium and the rovibrational model of the collision partner is examined and compared with the prior results for rubidium [9].

II. EXPERIMENT

The apparatus used to measure the spin-orbit energy transfer between the $6\,^2P_{3/2}$ and the $6\,^2P_{1/2}$ states is shown in Fig. 1 with the associated energy-level diagram. A Coherent MBR-110 Ti:sapphire ring laser was tuned to either 852 or 894 nm to prepare the $6\,^2P_{3/2}$ or the $6\,^2P_{1/2}$ states, respectively. The ring laser, which was pumped by a Coherent Verdi V-18 diode laser, has a linewidth less than 100 kHz with power less than 3.5 W. The hyperfine splitting of the ground $^2S_{1/2}$ state is 9.192 63 7 GHz and the laser was tuned to excite the $(F'' = 4)$

*afrl.rdlc.sci.org@kirtland.af.mil
†glen.perram@afit.edu

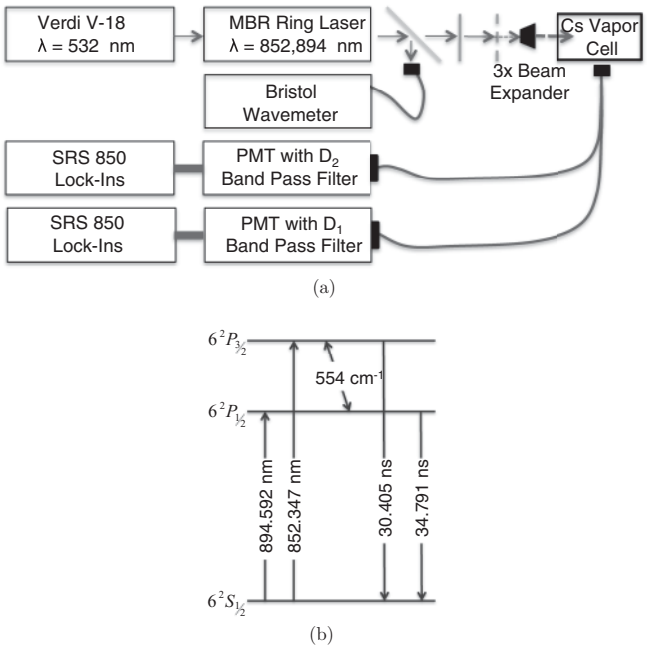

FIG. 1. Experimental apparatus to observe side fluorescence of cesium (a) with the associated energy level diagram (b).

component of the D_1 and D_2 transitions, at frequencies of $\nu_1 = 335\ 111$ GHz and $\nu_2 = 351\ 722$ GHz. These frequencies were actively monitored with a Bristol 621 laser wave meter to minimize laser drifting.

This beam was greatly attenuated ($< 4\ \mu$W), expanded to a diameter of 9.7 mm, and amplitude modulated before reaching the test cell. The resulting pump intensities were less than 5 μW/cm^2, significantly less than the saturation intensity. At low pressures the saturation intensity of the D_1 transition is approximately 2.5 mW/cm^2 [16]. Phase-sensitive detection with amplitude modulation at 100 Hz detection was employed to improve the signal-to-noise ratio.

Previously, the cell was described in detail and could sufficiently maintain and vary the cell temperature and pressure [17,18]. The single end of a bifurcated fiber bundle was placed perpendicular to the beam to observe the side fluorescence of the cell and was coupled into a pair of Hamamatsu photomultiplier tubes (R5509). Two ThorLabs bandpass filters centered near the D_1 [$\lambda = 890$ nm with a full width at half maximum (FWHM) of 10 nm] and D_2 ($\lambda = 850$ nm with a FWHM of 10 nm) transitions were used to limit the detection of out-of-band light to the two desired states. This allowed for the simultaneous monitoring of both the laser-prepared state and the collisionally populated satellite state, while continuously varying the pressure of buffer gas. Cell pressure was monitored with a MKS model 690A capacitance manometer with a range of 0–100 Torr. The cesium was 99.98% pure and all gases had a purity greater than 99.9% purity, with the one exception of HD, which had a purity of 97.3%. To avoid optical trapping, the cell was maintained at room temperature ($T = 298$ K), which resulted in a cesium vapor pressure of 1.5×10^{-6} Torr.

A small amount of scattered laser light was coupled into the photomultiplier tubes (PMTs). The level of the scattered light was measured by tuning slightly off resonance from the pump line while the cell contained no buffer gas. The scattered laser light was recorded to be less than 2% of the emission of the prepared state and was subtracted from the total observed signal. Additionally, the bandpass filter did not completely isolate the emission of the satellite state from the parent. The fraction of light passed through the satellite filter at the pump wavelength was measured to be less than 1% at zero buffer gas pressure, where no collisional transfer exists.

The observed intensities for both the D_1 and D_2 transitions, I_{D_1} and I_{D_2}, are linearly proportional to the concentration of the corresponding emitting states, N_1 and N_2:

$$I_{D_1} = [\mathrm{Cs}(^2\mathrm{P}_{1/2})]\mathrm{d}_1 = \mathrm{N}_1\mathrm{d}_1, \tag{1}$$

$$I_{D_2} = [\mathrm{Cs}(^2\mathrm{P}_{3/2})]\mathrm{d}_2 = \mathrm{N}_2\mathrm{d}_2, \tag{2}$$

where the proportionality constants, d_1 and d_2, depend on the spontaneous emission rates, detector response, and radiometric factors. The relative spectral response was initially $T_{D_1}/T_{D_2} = 0.70$ based on the transmission of the bandpass filters. The details of the spectral response calibration are developed in Ref. [19]. An improved value for the spectral response $d = d_1/d_2 = 0.98 \pm 0.19$, was achieved by assessing the resulting rates with respect to the principle of detailed balance.

III. RESULTS

Figure 2 shows the observed relative intensities from the D_1 and D_2 transitions converted to relative concentrations for N_1 and N_2, as the ethane or methane gas pressure is continuously increased. The ethane data in Fig. 2(a) was obtained during a period of less than 20 minutes while the pressure increased at an average rate of 80 mTorr/s, yielding greater than 25 000 samples. The methane data is more highly sampled at 124 000 samples over the 100 Torr range.

The signal for the satellite state initially increases linearly due to direct energy transfer. At higher pressures, collisional transfer back to the parent state begins to limit the satellite concentration and the ratio approaches a nearly statistical distribution.

In order to determine the rate of energy transfer from the observed intensity ratio, the following kinetic analysis is developed. First, laser excitation is used to populate either the $^2P_{1/2}$ or the $^2P_{3/2}$ via

$$\mathrm{Cs}(^2\mathrm{S}_{1/2}) + \mathrm{h}\nu_1 \xrightarrow{\mathrm{S}_1} \mathrm{Cs}(^2\mathrm{P}_{1/2}) \tag{3}$$

or

$$\mathrm{Cs}(^2\mathrm{S}_{1/2}) + \mathrm{h}\nu_2 \xrightarrow{\mathrm{S}_2} \mathrm{Cs}(^2\mathrm{P}_{3/2}), \tag{4}$$

where the rates S_1 and S_2 depend on the absorption cross section and the laser intensity. Second, the energy of the excited states is then transferred by collisions with the buffer gas, M:

$$\mathrm{Cs}(^2\mathrm{P}_{1/2}) + \mathrm{M} \underset{\mathrm{k}_{21}}{\overset{\mathrm{k}_{12}}{\leftrightarrow}} \mathrm{Cs}(^2\mathrm{P}_{3/2}) + \mathrm{M}, \tag{5}$$

with rate coefficients k_{12} and k_{21} to be determined in this work. Third, population of the excited state may return to the ground state via quenching or spontaneous emission:

$$\mathrm{Cs}(^2\mathrm{P}_{1/2}) + \mathrm{M} \xrightarrow{\mathrm{k}_{\mathrm{Q1}}} \mathrm{Cs}(^2\mathrm{S}_{1/2}) + \mathrm{M}, \tag{6}$$

$$\mathrm{Cs}(^2\mathrm{P}_{3/2}) + \mathrm{M} \xrightarrow{\mathrm{k}_{\mathrm{Q2}}} \mathrm{Cs}(^2\mathrm{S}_{1/2}) + \mathrm{M}, \tag{7}$$

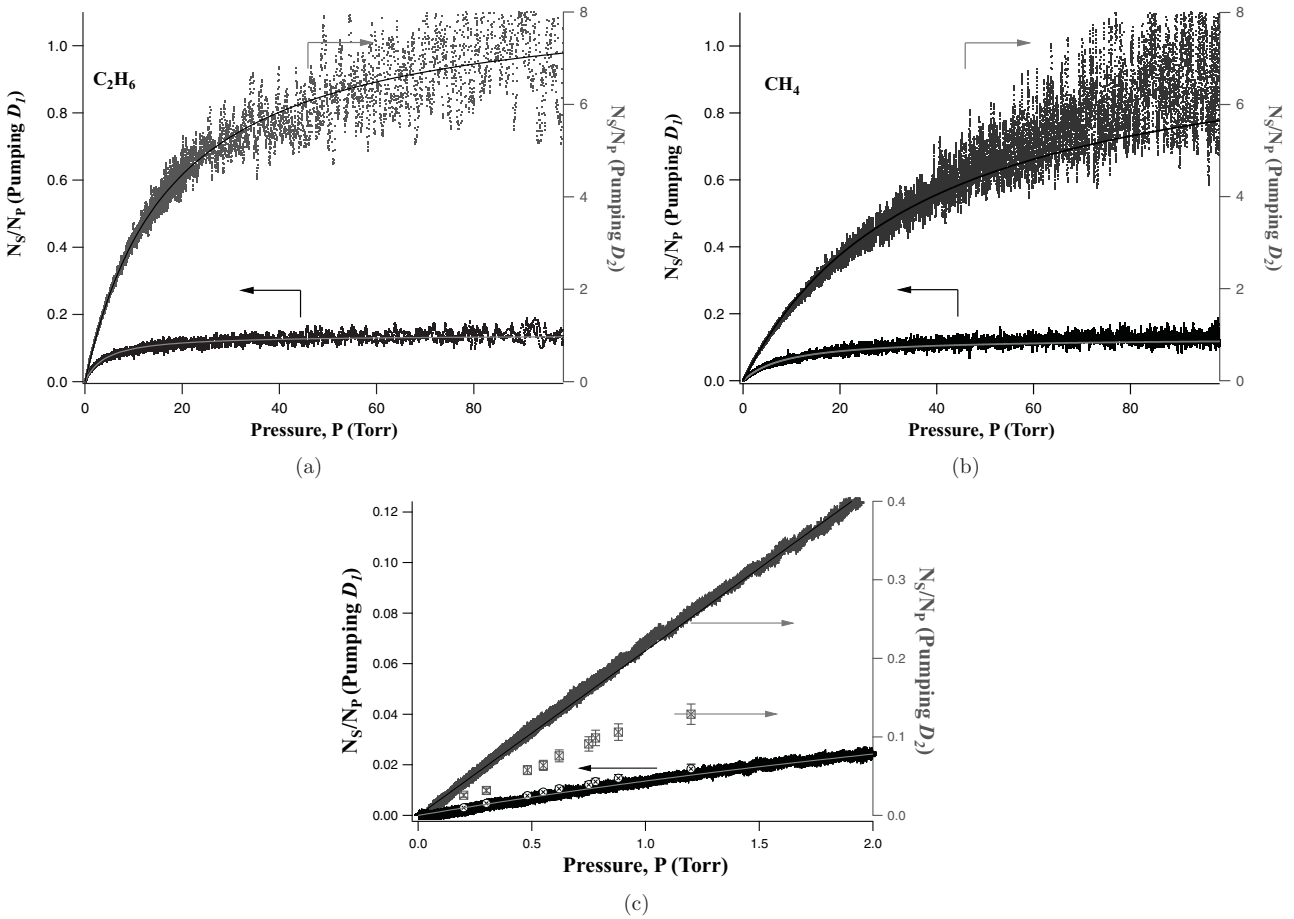

FIG. 2. Population ratios while preparing both the $^2P_{3/2}$ and $^2P_{1/2}$ states with varying pressure of (a) ethane and (b) methane with their corresponding fits to Eqs. (10) and (11). An expanded view of the methane data at low pressures is compared with the prior work (⊗, ☒) at 440 K (c) [7].

$$\mathrm{Cs}(^2\mathrm{P}_{1/2}) \xrightarrow{\mathrm{A}_1} \mathrm{Cs}(^2\mathrm{S}_{1/2}) + \mathrm{h}\nu_1, \tag{8}$$

$$\mathrm{Cs}(^2\mathrm{P}_{3/2}) \xrightarrow{\mathrm{A}_2} \mathrm{Cs}(^2\mathrm{S}_{1/2}) + \mathrm{h}\nu_2. \tag{9}$$

The quenching coefficients, k_{Q1} and k_{Q2}, depend slightly on the excited state. The radiative rates are $A_1 = 28.743 \times 10^6\ \mathrm{s}^{-1}$ and $A_2 = 32.889 \times 10^6\ \mathrm{s}^{-1}$ [16].

A steady-state analysis of the rate equations establishes the ratio of concentrations as

$$\left[\frac{N_1}{N_2}\right]_{\mathrm{pumpD_2}} = \left(\frac{I_{D_1}}{I_{D_2}}\right)\left(\frac{d_2}{d_1}\right) = \frac{k_{12}[M]}{A_1 + (k_{Q1} + k_{21})[M]}, \tag{10}$$

$$\left[\frac{N_2}{N_1}\right]_{\mathrm{pumpD_1}} = \left(\frac{I_{D_2}}{I_{D_1}}\right)\left(\frac{d_1}{d_2}\right) = \frac{k_{21}[M]}{A_2 + (k_{Q2} + k_{12})[M]}, \tag{11}$$

when pumping the D_2 and D_1 transitions, respectively.

A least-squares fit of Eqs. (10) and (11) to the observed population ratios are shown in Fig. 2. The resulting fit parameters are reported as the spin-orbit and quenching cross sections in Table I. The average relative speed is defined as

$$\bar{v} = \sqrt{\frac{8k_BT}{\pi\mu}}, \tag{12}$$

where μ is the reduced mass of the collision pair, T is the gas temperature, and k_B is Boltzmann's constant. The thermally averaged rate coefficients

$$k(T) = \int_0^\infty \sigma(v)\, v f(v;T)\, dv \cong \sigma\bar{v} \tag{13}$$

are related to the energy-dependent collision cross section, $\sigma(v)$, and Maxwellian relative speed distribution, $f(v)$. For a collision cross-section independent of energy, the rate coefficient is simply the product of the cross section and the average relative speed. The error bounds reported in Table I reflect only the statistical errors as determined by one standard deviation in the corresponding fit parameter.

The ratio of the forward and the reverse spin-orbit rates must obey the principle of detailed balance:

$$\frac{k_{21}}{k_{12}} = \frac{\sigma_{12}}{\sigma_{21}} = \frac{g_2}{g_1} e^{-\Delta E_{\mathrm{so}}/k_BT} = f, \tag{14}$$

TABLE I. Cross sections for the energy transfer from the $^2P_{3/2}$ to the $^2P_{1/2}$ levels of cesium induced by collisions at 298 K.

Collisional artner	Cross sections (Å^2)		Ratio σ_{12}/σ_{21}	Temp. (K)	Ref.
	σ_{21}	σ_{12}			
N_2	16.32 ± 0.03	1.81 ± 0.01	11.09 ± 0.82%	298	This work
	16.2 ± 2	3.6 ± .5	22 ± 4%	313	[4]
	25.0 ± 2.5	4.7 ± 0.5	19 ± 2.7%	315	[5]
H_2	34.11 ± 0.04	4.43 ± 0.01	13.00 ± 0.91 %	298	This work
	29.6 ± 4.4	6.5 ± 1	22 ± 5%	313	[4]
	44 ± 4.4	6.7 ± .5	15.2 ± 1.9%	315	[5]
	25.8 ± 2.58	3.6 ± .4	14.0 ± 2.1%	300	[8]
HD	30.01 ± 0.05	4.09 ± 0.01	13.62 ± 0.95 %	298	This work
	32 ± 3.2	4.8 ± 0.5	15.0 ± 2.2%	315	[5]
	22.5 ± 2.25	3.9 ± 0.4	17.3 ± 2.5%	300	[8]
D_2	22.69 ± 0.02	3.02 ± 0.01	13.31 ± 0.93 %	298	This work
	28 ± 2.8	4.2 ± 0.4	15.0 ± 2.1%	315	[5]
	16.4 ± 1.6	2.3 ± 0.2	14.0 ± 1.6%	300	[8]
CH_4	21.36 ± 0.01	2.95 ± 0.01	13.82 ± 0.96 %	298	This work
	16.8 ± 1.7	2.3 ± 0.2	13.7 ± 1.83%	298	[7]
CF_4	65.56 ± 0.06	13.26 ± 0.01	20.23 ± 1.04%	298	This work
	52.0 ± 5.2	7.9 ± 0.8	15.2 ± 2.2%	310	[7]
C_2H_6	64.81 ± 0.08	9.70 ± 0.01	14.97 ± 0.84%	298	This work
	57.5 ± 5.8	7.9 ± 0.8	13.7 ± 2.0%	298	[8]
C_2F_6	137.53 ± 0.08	16.28 ± 0.01	11.84 ± 0.84%	298	This work

where the degeneracies are $g_2 = 4$ and $g_1 = 2$ and the spin-orbit splitting is $\Delta E_{so} = 554\ \text{cm}^{-1}$. Constraining the average value for this ratio for all collision partners to $f = 0.132$ at $T = 298$ K provides an improved measure of the relative detectivity, $\frac{d_1}{d_2} = 0.979 \pm 0.186$. The observed ratios $\frac{\sigma_{12}}{\sigma_{21}}$ range between 0.12–0.16, suggesting a systematic error of about 15%. Note that the prior determination of the spin-orbit relaxation rates exhibit greater violations of detail balance.

The curvature at higher pressures observed in Fig. 2 reflects the combined contributions of the reverse spin-orbit rate and quenching rate, as expressed in the denominator of Eqs. (10) and (11). Any difference between the high pressure asymptotic limit and the detail balance ratio of Eqs. (14) implies a significant quenching rate. These expected asymptotic values for pumping the D_2 transition when no quenching is present is $1/f = 7.58$. Utilizing the limits, one can compute the quenching rate for each of the gases measured noting that as quenching increases, the limiting value decreases. As shown in Table II, the quenching for nitrogen is the greatest and is followed by that of the H_2, HD, and D_2. These four rates have previously been measured and follow closely the trend shown in Table II [5]. The error bounds reported in Table II reflect only the statistical uncertainty in the asymptotic limit. The larger systematic errors of ≈15% discussed for the spin-orbit rates imply that the lower quenching rate represents an upper bound. For example, the ethane asymptotic limit of 6.2 is nearly compatible with $1/f = 7.58$ and thus exhibits little to no quenching.

Hexafluoroethane, C_2F_6, exhibits the largest spin-orbit relaxation rate of the current gasses studied. The corresponding quenching rate is marginally faster than ethane. This shows for a DPAL system that hexaflouroethane may be ideal in terms of quenching and spin-orbit rates. No decomposition of C_2F_6 was observed in the course of this investigation, however, these studies were performed at room temperature with very low laser intensities which are not typical DPAL system conditions.

TABLE II. Quenching rates from D_2 pumping.

Buffer gas	$\frac{k_{21}}{k_{12}+k_{Q_1}}$	σ_{Q1}	Previous work	Ref.
C_2H_6	6.19 (±0.29)	2.2 (±0.6)		
C_2F_6	5.43 (±0.28)	6.4 (±1.2)		
CH_4	5.12 (±0.68)	1.4 (±0.6)		
CF_4	4.16 (±0.55)	11 (±3)		
H_2	3.45 (±0.29)	5.3 (±0.8)	7 (±2) Å^2	[5]
HD	2.78 (±0.24)	7(±1)	4 (±1) Å^2	[5]
D_2	3.09 (±0.25)	4.4 (±0.6)	8 (±3) Å^2	[5]
N_2	0.38 (±0.03)	34 (±3)	69 (±4) Å^2	[5]

IV. DISCUSSION

The spin-orbit mixing rates are usually enhanced when they have a resonant path for the energy exchange. Only electronic to translational energy exchange is available with cesium–rare-gas collisions [2]. The temperature dependence of the cesium–rare-gas energy transfer is not observed in the complex molecules of Walentynowicz, suggesting that the molecules may transfer the energy by rovibrational pathways [7,8].

Rotondaro suggested the possibility for accessing the rotational states of the buffer gas for the spin-orbit relaxation of rubidium [9]. The spin-orbit splitting in rubidium of 237.6 cm^{-1} is less than for cesium which has an energy defect of 554 cm^{-1}. Cesium may be able to access some of the lower

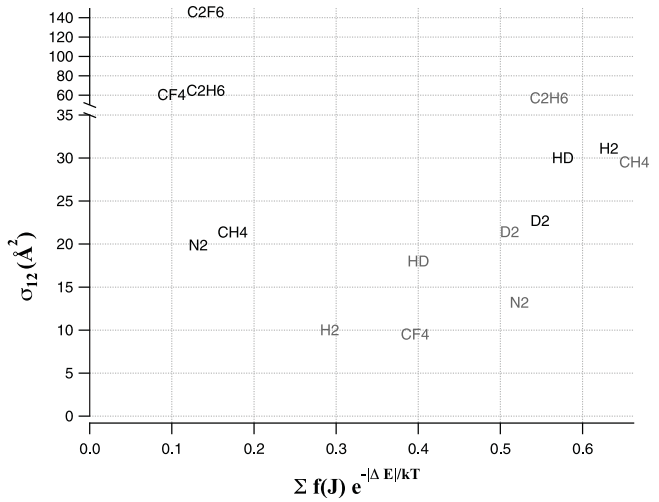

(a)

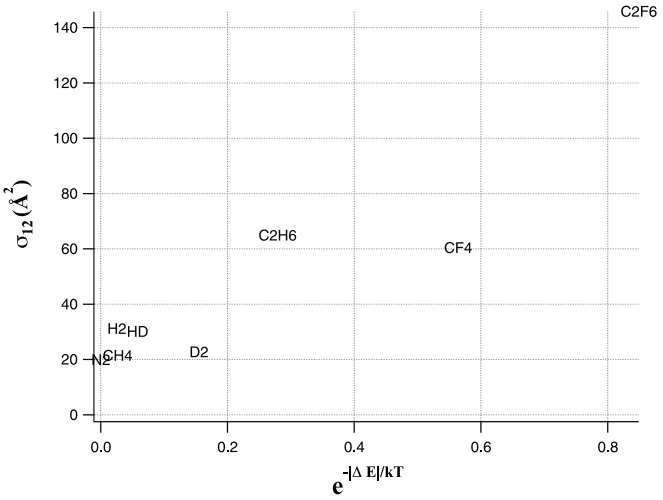

(b)

FIG. 3. Demonstrations of the possible energy exchange between electronic to rotational, where $F(J) = \frac{hcB_v}{k_BT}(2J+1)e^{hcB_vJ(J+1)/k_BT}$ (a) and electronic to vibrational (b) with inclusion of data from Rotondaro in gray [9].

vibrational states of the more complex molecules. Rotondaro used the general reaction model

$$A(^2P_{3/2}) + M(J'') \rightleftharpoons A(^2P_{1/2}) + M(J'), \qquad (15)$$

where $A(^2P_{x/2})$ represents the alkali-metal atom and $M(J)$ represents the molecular collision partner in rotational level J. He demonstrated a correlation between Rb and the total energy defect of the rotating buffer gas [9]. The correlation expressed by Rotondaro utilized the relation

$$k_{E-R} = \sum_J e^{-|\Delta E|/k_BT}\frac{hcB_v}{k_BT}(2J+1)e^{hcB_vJ(J+1)/k_BT}, \qquad (16)$$

where k_{E-R} is the electronic-to-rotational energy exchange rate, ΔE is the difference on the alkali-metal energy defect from the rotational energy defect, B_v is the rotational constant, and J is the rotational state. Figure 3 places the current results for cesium in the context of this prior work for rubidium.

As one can see, the rubidium correlation seems to fit nicely, and the cesium cross sections seem to follow a similar trend, with the exception of ethane and carbon tetraflouride. While these molecules have the smaller theoretical electronic energy exchange rate, they have the largest cross sections.

Walentynowicz noted that carbon tetraflouride has a set of vibrational states (437 and 635 cm^{-1}) that are close to the energy defect for cesium [7]. This leads one to believe that the energy is not being transferred to the rotational states as in the other cases but instead into a vibrational state. Ethane has vibrational states (289 and 822 cm^{-1}) that have the same magnitude as the energy defect of cesium, and hexafluoroethane has vibrational states at 520 and 619 cm^{-1}. The relationship for electronic-vibrational energy transfer is shown in Fig. 3(b). The hydrides appear to achieve a maximum for the correlation to electronic-rotational transfer at 30 Å^2. The correlation for electronic-to-vibrational energy transfer CF_4 and C_2F_6 achieve a maximum ranging from 60 to 130 Å^2. It appears easier to access vibrational states over the rotational states of the collisional partner.

V. CONCLUSION

The collision-induced mixing of the 6 $^2P_{1/2,3/2}$ levels of atomic cesium by molecular partners has been revisited, and new rates have been reported to support the development of diodepumped alkali-metal lasers. The results further support a rovibrational energy-transfer mechanism for enhancing these rates. Hexafluoroethane offers the faster relaxation rate with modest quenching and might be explored as a buffer gas in optically pumped cesium lasers.

ACKNOWLEDGMENTS

Support for this work from the Air Force Office of Scientific Research and the High Energy Laser Joint Technology Office is gratefully acknowledged. In addition, I would like to thank Matt Lange and Doug Wertepny for their help with the preliminary work on this project.

[1] L. Krause, Appl. Opt. **5**, 1375 (1966).
[2] A. Gallagher, Phys. Rev. **172**, 88 (1968).
[3] M. Czajkowski and L. Krause, Can. J. Phys. **43**, 1259 (1965).
[4] D. A. McGillis and L. Krause, Phys. Rev. **153**, 44 (1967).
[5] D. A. McGillis and L. Krause, Can. J. Phys. **46**, 1051 (1968).
[6] M. Czajkowski, D. A. McGillis, and L. Krause, Can. J. Phys. **44**, 91 (1966).
[7] E. Walentynowicz, R. A. Phaneuf, W. E. Baylis, and L. Krause, Can. J. Phys. **52**, 584 (1974).
[8] E. Walentynowicz, R. A. Phaneuf, and L. Krause, Can. J. Phys. **52**, 589 (1974).
[9] M. D. Rotondaro and G. P. Perram, Phys. Rev. A **57**, 4045 (1998).
[10] W. Krupke, R. Beach, V. Kanz, and S. Payne, Opt. Lett. **28**, 2336 (2003).

[11] R. J. Beach, W. F. Krupke, V. Kanz, S. Payne, M. Dubinskii, and L. Merkle, J. Opt. Soc. Am. B **21**, 2151 (2004).
[12] A. L. Schawlow and C. H. Townes, Phys. Rev. **112**, 1940 (1958).
[13] R. H. Page, R. J. Beach, V. K. Kanz, and W. F. Krupke, Opt. Lett. **31**, 353 (2006).
[14] B. Zhdanov, T. Ehrenreich, and R. Knize, Opt. Commun. **260**, 696 (2006).
[15] J. Zweiback, G. Hager, and W. Krupke, Opt. Commun. **282**, 1871 (2009).
[16] D. A. Steck [http://steck.us/alkalidata].
[17] G. A. Pitz, D. E. Wertepny, and G. P. Perram, Phys. Rev. A **80**, 062718 (2009).
[18] G. A. Pitz, C. D. Fox, and G. P. Perram, Phys. Rev. A **82**, 042502 (2010).
[19] M. D. Rotondaro, *Collisional Dynamics of the Rubidium* 5^2P *Levels*, Ph.D. thesis, Air Force Institute of Technology, 2950 Hobson Way WPAFB, OH 45433-7765 (1995).